ACS APPLIED MATERIALS & INTERFACES

Research Article

www.acsami.org

Dual-Layer Nanostructured Flexible Thin-Film Amorphous Silicon Solar Cells with Enhanced Light Harvesting and Photoelectric Conversion Efficiency

Yinyue Lin,[†,‡,¶] Zhen Xu,[‡,§,¶] Dongliang Yu,[‡] Linfeng Lu,[‡] Min Yin,[‡] Mohammad Mahdi Tavakoli,[⊥] Xiaoyuan Chen,[‡] Yuying Hao,[†] Zhiyong Fan,[⊥] Yanxia Cui,[*,†] and Dongdong Li[*,‡]

[†]Key Lab of Advanced Transducers and Intelligent Control System of Ministry of Education, College of Physics and Optoelectronics, Taiyuan University of Technology, Taiyuan 030024, China

[‡]Shanghai Advanced Research Institute, Chinese Academy of Sciences, 99 Haike Road, Zhangjiang Hi-Tech Park, Pudong, Shanghai 201210, China

[§]University of Chinese Academy of Sciences, Beijing 100039, China

[⊥]Department of Electronic and Computer Engineering, The Hong Kong University of Science and Technology, Clear Water Bay, Kowloon, Hong Kong SAR, China

Supporting Information

ABSTRACT: Three-dimensional (3-D) structures have triggered tremendous interest for thin-film solar cells since they can dramatically reduce the material usage and incident light reflection. However, the high aspect ratio feature of some 3-D structures leads to deterioration of internal electric field and carrier collection capability, which reduces device power conversion efficiency (PCE). Here, we report high performance flexible thin-film amorphous silicon solar cells with a unique and effective light trapping scheme. In this device structure, a polymer nanopillar membrane is attached on top of a device, which benefits broadband and omnidirectional performances, and a 3-D nanostructure with shallow dent arrays underneath serves as a back reflector on flexible titanium (Ti) foil resulting in an increased optical path length by exciting hybrid optical modes. The efficient light management results in 42.7% and 41.7% remarkable improvements of short-circuit current density and overall efficiency, respectively. Meanwhile, an excellent flexibility has been achieved as PCE remains 97.6% of the initial efficiency even after 10 000 bending cycles. This unique device structure can also be duplicated for other flexible photovoltaic devices based on different active materials such as CdTe, Cu(In,Ga)Se_2 (CIGS), organohalide lead perovskites, and so forth.

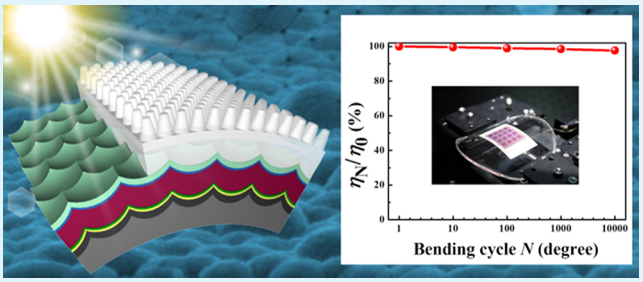

KEYWORDS: *thin-film solar cells, flexible, nanopillar membrane, broadband and omnidirectional performances, shallow dent arrays*

INTRODUCTION

Hydrogenated amorphous silicon thin-film solar cell (*a*-Si:H TFSC) is a promising alternative to its crystalline silicon wafer-based counterparts due to the cost reduction and shorter energy-payback time.[1] Moreover, thin-film solar cells constructed on flexible substrates offer new opportunities for building-integrated photovoltaics (PVs) and portable power sources because of their lightweight, mechanical flexibility.[2,3] It is known that the performance of PV devices largely relies on their optical absorption and carrier collection dynamics in the devices. The *a*-Si:H material has relatively poor transport properties, with the minority carrier diffusion length of around 300 nm or less,[4] and it also demonstrates significant light induced efficiency degradation, known as the Staebler–Wronski (S–W) effect.[5,6] Using thinner absorbing layers will improve effective carrier transport and reduce the impact of the S–W degradation at 10–15% of initial efficiency,[7,8] but it will simultaneously sacrifice light absorption. In this regard, the strategies for designing state-of-the-art light harvesting structures have become an intriguing topic to solve the fundamental incompatibility between electronics and optics in the PV devices.

It has been discovered that three-dimensional (3-D) nanostructure can substantially improve the power conversion efficiency (PCE) via various light trapping mechanisms.[9,10] A number of nanostructures, such as nanopillars,[11] nanotubes,[12,13] nanodomes,[14] nanocones,[15] nanowells,[16] nanodents,[17−19] nanospikes,[20,21] and hierarchical architecture,[22] etc., have been fabricated. In addition, the effective performance improvements have been widely demonstrated based on different material

Received: February 22, 2016
Accepted: April 7, 2016
Published: April 7, 2016

DOI: 10.1021/acsami.6b02194
ACS Appl. Mater. Interfaces 2016, 8, 10929−10936

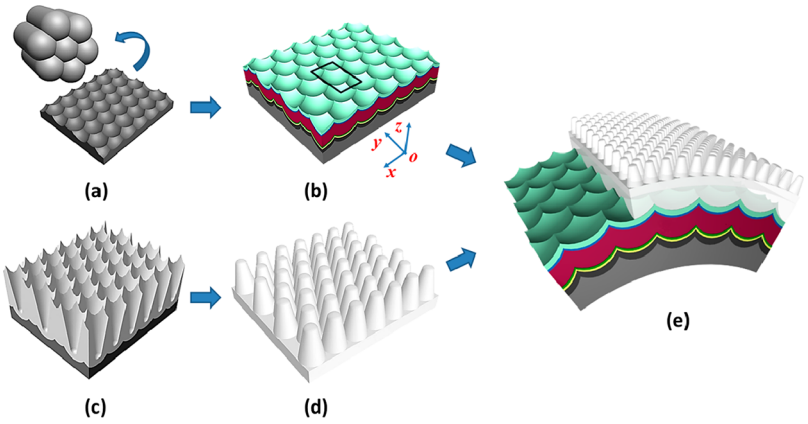

Figure 1. Schematic process of fabricating *a*-Si:H TFSCs on flexible Ti substrate with dual-interfacial patterned structure. (a) Ti substrate with nanodent arrays after removal of TONT layer. (b) An *a*-Si:H TFSC constructed on the pattern Ti substrate. The black rectangle shows the unit cell of the patterned structure. (c) V-shape AAO thin films obtained by multistep anodic oxidation process. (d) Nanopillar membrane obtained by molding process, which can be directly peeled from AAO template. (e) A flexible solar cell on pattern Ti foil covered with PDMS nanopillar membrane.

systems. One straightforward method is to form antireflection (AR) films on the upper surface of front window without paying the price of reducing electrical performance. Flexible plastics decorated with geometry controlled 3-D nanocone or nanopillar arrays have been developed as AR films.[23,24] Benefiting from the gradually changed effective refractive index from the top of the nanostructure to the bulk material, broadband and omnidirectional enhanced light absorption and PCE were achieved. The AR films can be readily attached onto various substrates for both rigid and flexible solar cells. In the case of solar cells with substrate configuration, improved light harvesting can be rationally achieved on nanotextured back reflector by exciting various optical modes.[14,17,21,25] Conventional fabrication approaches for nanostructured back reflector largely rely on costly nanofabrication on rigid substrates with limited scalability. We recently reported *a*-Si:H TFSCs built on flexible aluminum (Al) foils with organized nanopatterns utilizing cost-effective electrochemical anodization.[17−19] A distinct performance was realized, which is even better than the device on conventional random textured substrate.[17] A variety of 3-D back reflectors with precisely tuned pitch and height (or depth) were subsequently developed with remarkably improved broadband absorption.[20,21,25] Further increase of the aspect ratio will benefit a higher light absorption capability especially for short wavelengths, where the antireflection effect dominates light absorption.[20,25] However, the increased structural aspect ratio leads to undesirable film nonuniformity, which in turn will hurt both short circuit current density (J_{SC}) and open circuit voltage (V_{OC}) due to the deterioration of the internal electric field and carrier collection capability. As a result, the optimized 3-D back reflectors typically have a moderate aspect ratio to depress the materials defect density and carrier recombination.[20]

In this work, we report flexible *a*-Si:H TFSCs built on flexible titanium (Ti) foil with nanodent (ND) texture fabricated by cost-effective Ti anodization. Compared to its Al counterpart, Ti possesses lower coefficient of thermal expansion, higher plastic deformation resistance, and temperature tolerance. To further reduce the light reflection at air/device interface, a flexible 3-D nanopillar membrane fabricated by casting polydimethylsiloxane (PDMS) into porous anodic alumina was attached onto device surface as an AR skin. Solar cell based on the dual-layer patterned nanostructures has demonstrated a PCE of 8.05% under AM 1.5 irradiation, which outperforms the planar counterpart by 41.7%. More intriguingly, the PV devices showed superior omnidirectional performance owing to the 3-D nanopillar AR skin and excellent flexibility. These results can be extended to rational design of a wide range of high efficiency flexible solar cells, including CdTe, Cu(In,Ga)Se_2, perovskite-based technologies.

EXPERIMENTAL SECTION

Preparation and Fabrication. *Preparation of Patterned Ti Substrates.* Ti foils (99.7%, 200 μm thickness) were first cleaned in acetone, ethanol, and deionized (DI) water each for 15 min. Then the Ti foils were chemically polished for 30 s at room temperature in a solution of hydrofluoric acid, nitric acid, and DI water with volume ratios of 1:1:2.[26] The anodization was carried out under 170 V (3 °C) for 1 h in ethylene glycol electrolyte containing 0.3 wt % NH_4F and 12 vol % DI water.[27] Self-organized TiO_2 nanotubes (TONTs) were obtained, under which nanodent arrays were formed on the Ti foils. The oxide layers were subsequently removed from the Ti foil by adhesive tape,[28] which left the nanodent array on the flexible substrate with an average pitch size (center-to-center distance) of ∼600 nm.

Fabrcation of a-Si:H Solar Cells. The *a*-Si:H TFSCs were fabricated on the patterned Ti substrates. Specifically, a 100 nm thick Ag layer was deposited as a back reflector on the patterned Ti substrate by DC magnetron sputtering. Then an aluminum doped zinc oxide (AZO) spacer layer, with a thickness of 30 nm, was prepared on the Ag-coated substrate by radio frequency (RF) magnetron sputtering of a 2 wt % Al_2O_3 doped ZnO ceramic target (purity 99.99%). Subsequently, a stack of *n-i-p* silicon layers was successively fabricated in a plasma enhanced chemical vapor deposition (PECVD) multichamber system. The *n*- and *p*-type layers are 20 and 10 nm thick, respectively, while the thickness of the intrinsic *a*-Si:H layer is 280 nm. An 80 nm indium-doped tin oxide (ITO) top contact, which also serves as a part of antireflection coating, was deposited by RF sputtering. Finally, an Ag grid was evaporated as the top electrode over ITO using a contact mask at room temperature.[17,19,25] For comparison, a solar cell was also fabricated on a flat glass substrate under the same process, serving as a planar control device.

Fabrication of PDMS Membranes. PDMS membranes with nanopillar arrays were produced from V-shape anodic aluminum oxide (AAO) templates. In brief, high purity aluminum (99.999%) foils were first anodized in 0.3 M oxalic acid solution at 40 V (5 °C) for 2 h. The as-formed porous oxide layers were then completely removed in a mixed solution of 1.8 wt % CrO_3 and 6 wt % H_3PO_4 at 60 °C for 3 h. The following anodization was then performed in the

DOI: 10.1021/acsami.6b02194
ACS Appl. Mater. Interfaces 2016, 8, 10929−10936

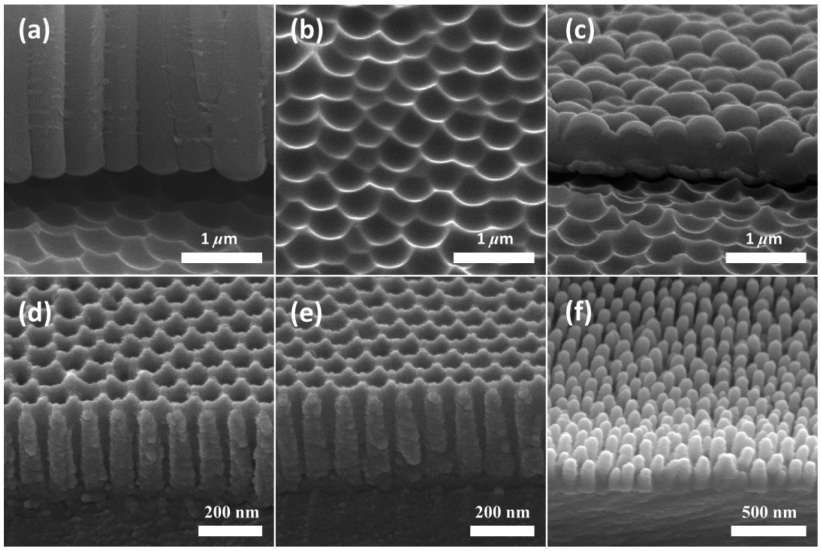

Figure 2. SEM characterizations of (a) TONT film, (b) nanodent arrays on Ti foil, (c) *a*-Si:H TFSCs on nanopatterned Ti substrate, V-shape AAO templates (d) before and (e) after antistick coating, and (f) top surface of composite PDMS membrane covered with nanopillar arrays.

same electrolyte solution at 40 V (5 °C) for 30 s. Subsequently, the samples were transferred into a 5 wt % H_3PO_4 solution at 30 °C for 6 min to widen the as formed holes. The V-shape AAO will be obtained after five cycles anodization and widen processes. Then an antisticking coating process using a fluorinated silane precursor was adopted on the templates by a molecular vapor deposition (MVD) method (Molecular-100S, Nanocarve Ltd.).

Thermal-curable high modulus polydimethylsiloxane (*h*-PDMS) as the replicated layer was first spin-coated on the V-shape AAO template, and sequentially Sylgard 184 PDMS as a scaffold layer was poured on to form a composite film[29] followed by a solidification in a drying oven at 60 °C for 3 h. Then the composite PDMS membrane (~2 mm in thickness) with nanopillared top surface was obtained by peeling it off from the template and could be readily transferred onto the photovoltaic device as a flexible AR window (Figure 1e).

Simulations. The finite difference in time domain (FDTD) method was employed to investigate the optical properties of solar cells. The unit cell of the patterned structure (see the black rectangle in Figure 1b) was set as the simulation region using period boundary conditions in the *x*-axis and *y*-axis and perfectly matched layer (PML) boundary conditions in the *z*-axis. The device is normally irradiated by a plane wave light source with the electric and magnetic components polarized along the *x* and *y* axes, respectively. One monitor is placed between the source plane and device surface to detect the device absorption. Moreover, mesh grids with a 2 nm minimized side length were applied in the simulations so that the electromagnetic field distributions could be calculated accurately. Complex refractive indices of Ag and Ti are adopted from Palik's handbook of Optical Constants,[30] while those of AZO, ITO, and *n-i-p* *a*-Si:H are our measured data as shown in Figure S1.

RESULTS AND DISCUSSION

Figure 1, panels a and b illustrate the fabrication process of thin-film solar cells on patterned Ti substrates. Self-organized TiO_2 nanotubes were first formed on flexible Ti foils by a low-cost and scalable anodization in an ethylene glycol solution under 170 V. Ti foil with ND arrays (Figure 1a) will be disclosed by subsequent removal of the oxide layer using adhesive tape. The *a*-Si:H TFSC will be constructed onto the nanotextured foil by a series of vapor depositions. PDMS membranes with nanopillar arrays were fabricated from V-shape anodic aluminum oxide (AAO) templates (Figure 1c,d),[25,31,32] and they can be readily transferred onto the photovoltaic device as a flexible AR window (Figure 1e). The details of the processes can be found in the Experimental Section.

In previous work,[17] Al foils with nanometer-sized shallow dent arrays have been successfully demonstrated by removing the porous AAO films, which were obtained via large scale and low cost electrochemical anodization. Because of the similar morphologies and anodizing process, the growth mechanisms of AAO have been transplanted to interpret the formation of the tubular structure in TONT films.[33] Thereby, the ND arrays are also expected to be formed underneath the TONT films. Figure 2, panel a shows a tilted view of a TONT film in which vertically aligned one-dimensional nanotubes are observed. Large scale Ti ND arrays with an average pitch size (center-to-center distance) of ~600 nm (Figure 2b), and a depth of ~200 nm (Figure S2), appeared after removal of the nanotubes. After depositing all the functional layers of *a*-Si solar cells (Figure 2c), a morphological evolution from nanodents to nanodomes can be observed due to the shade effect in the deposition process. Although the shape of nanodent has not been retained very well after completing the device fabrication, the nanodome structure in fact works well on increasing optical path length by inducing guided modes and plasmonic modes.[14,17] Our previous results also indicated that further increasing the aspect ratio will lead to a significant film nonuniformity, which can substantially depress the device performance due to the deterioration of the internal electric field and carrier collection capability.[20,25]

The nanopillar arrays on PDMS membrane are formed by template process from V-shape AAO molds. Figure 2, panel d shows a tilted view of V-shape AAO template formed by multistep anodization. The interpore distance and pore depth are 100 and 250 nm, respectively. Note that these geometries can be effectively tuned in a large scale by adopting different electrolytes and bias voltages.[34,35] After antisticking treatment by a MVD process, a uniform perfluorodecylytrichlorosilane (FDTS) thin layer is conformally coated onto the V-shape nanostructure (Figure 2e). Figure 2, panel f shows the obtained composite PDMS nanopillars with an average pitch size and height of 100 and 120 nm, respectively. This height mismatch compared with the template pore depth is ascribed to the relatively low modulus of the *h*-PDMS (~9 MPa), which limits

DOI: 10.1021/acsami.6b02194
ACS Appl. Mater. Interfaces 2016, 8, 10929−10936

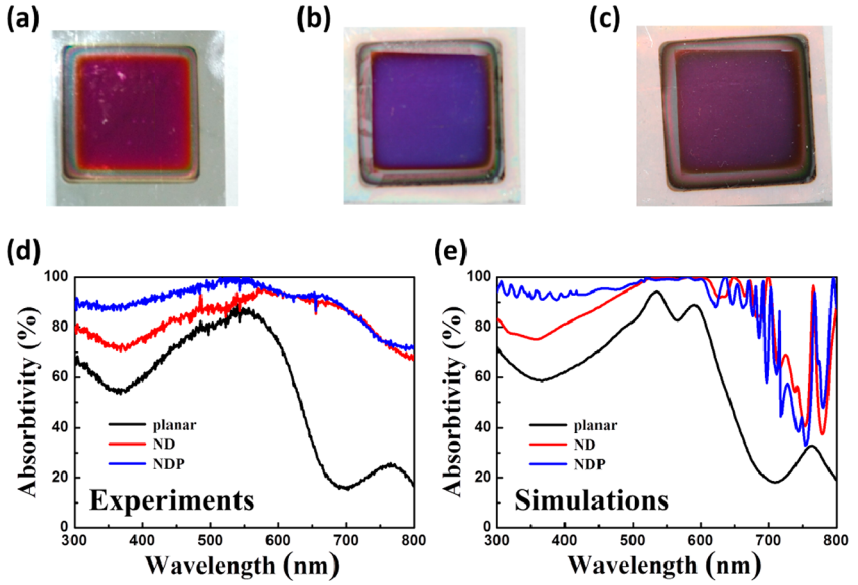

Figure 3. Photographs of (a) planar and (b, c) nanodent solar cells covered (b) without and (c) with PDMS nanopillars membrane. (d) Measured and (e) calculated absorption spectra of the above three devices.

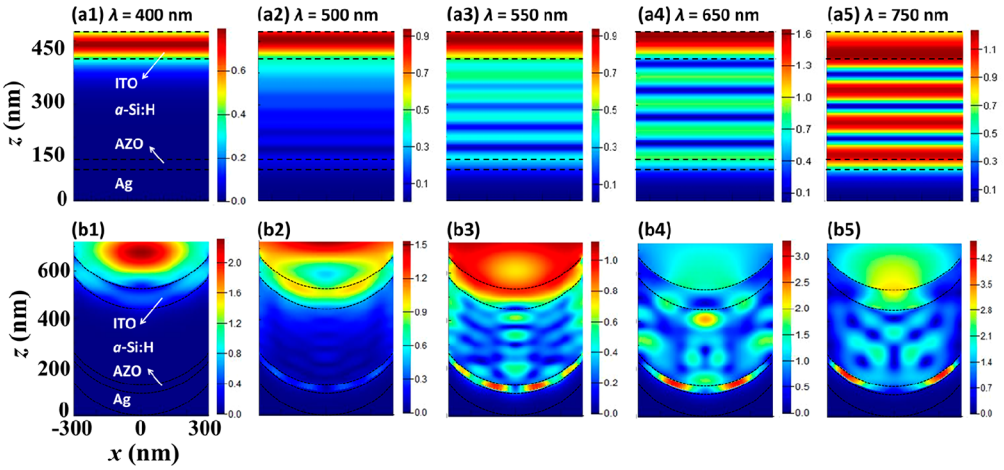

Figure 4. Electric field (|*E*|) distributions in (a1−a5) planar device and (b1−b5) patterned device at wavelengths of (a1, b1) 400 nm, (a2, b2) 500 nm, (a3, b3) 550 nm, (a4, b4) 650 nm, and (a5, b5) 750 nm, respectively. The black dashed lines represent the outline of the each layer.

the replication of small feature size at the template pore bottom.[36]

To investigate the antireflective properties of the patterned substrate, devices on both planar substrate and patterned Ti substrate with ND arrays are fabricated. Figure 3, panels a and b display the photographs of the two different devices. An evolution from bright red to dark blue can be observed as the devices changed from a planar substrate to a patterned one. To quantitatively investigate the optical properties of the devices, UV−vis reflection measurements were carried out with an integrating sphere. Figure 3, panel d presents the normal incident absorption spectra of the nanostructured devices as well as the flat reference cell. The ND device represents a much higher absorption capability than the flat device over the whole wavelength region. The observed phenomenon is expected because the patterned solar cell could not only reduce the reflection in short wavelength due to the nanotextured top surface, but also trap long wavelength light by introducing surface plasmon modes and other photonic modes.[17,19]

To verify experimental observations, the absorption spectra have been calculated by employing the FDTD method. The simulation results display a consistent trend with the experimental ones in the full wavelength range as shown in Figure 3, panel e. The noticeable oscillation in the long wavelength region on the patterned devices can be ascribed to the strong resonances occurring in the perfectly ordered structures in the simulation model.[17,19] Despite these deviations, the overall simulation results reproduce the experimental trends very well, which encourage us to further study the field distributions within the absorbing layer to understand the light propagation in nanostructured devices. Figure 4 presents the distributions of electric field (|*E*|) at different wavelengths, namely from left to right, λ = 400 nm, 500 nm, 550 nm, 650 nm, and 750 nm, respectively. The corresponding magnetic field (|*H*|) distributions are also plotted in the Supporting Information (Figure S3). Figure 4, panel a1 indicates that a significant portion of incident light (λ = 400 nm) is reflected back toward the incident space and results in interference patterns along *z* direction outside the *a*-

DOI: 10.1021/acsami.6b02194
ACS Appl. Mater. Interfaces 2016, 8, 10929−10936

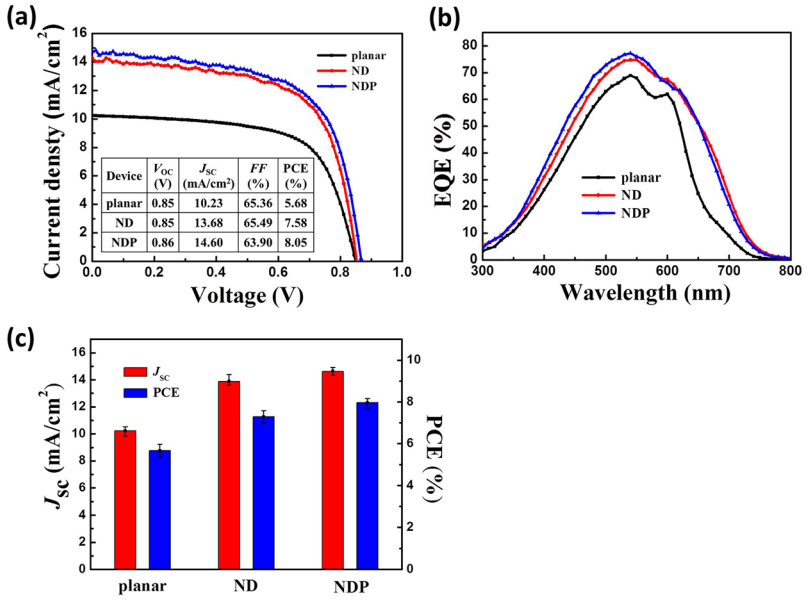

Figure 5. (a) $J-V$ curves under AM 1.5 irradiation (100 mW/cm^2) and (b) EQE of three different *a*-Si:H TFSCs; the inserted table in panel a shows the electrical performances of the three devices. (c) The J_{SC} and PCE values as a function of device configurations.

Si:H layer for a planar device. In the case of nanopatterned solar cell, the interference happens along both z and x directions. Thus, the 2-D interference forms circular shaped mode as displayed Figure 4, panel b1, which benefits light trapping than the planar one. However, there is still ∼20% reflection loss at 400 nm (see Figure 3d) due to the relatively low aspect ratio in comparison with the 3-D nanostructures.[25] The electromagnetic field distributions (Figure 4b1 and Figure S2b1) also indicate that the light absorption is mainly contributed by the top layer of *a*-Si:H and ITO top contact.

As the incident wavelength becomes longer, the electric field intensity within *a*-Si layers is more evident. It is observed that the light is strongly confined in the patterned device instead of forming interference fringes (Figure 4a2−a5 and Figure S3a2−a5), which cannot be effectively trapped within the absorption layer. The complex field patterns formed at different wavelengths (Figure 4b2−b5 and Figure S3b2−b5) shares the following common features. First, in the *a*-Si:H layer, very complicated filed patterns are formed, which can be regarded as a hybridization of oscillating modes along the vertical direction and those along the horizontal direction.[37] The constructive modes formed along the vertical direction are also defined as the cavity modes, originated from the refractive index change between different layers, which also exist in the flat device. The constructive modes formed along the horizontal direction belong to Bloch modes, which are generated due to the periodical property of the structure (i.e., the lattice scattering effect).[37,38] It was observed that the numbers of both cavity modes and Bloch modes decrease as the wavelength becomes longer. Second, in the AZO part, there is strong intensity of electric field and the number of the oscillation modes also decreases when the wavelength becomes larger. In this double interface structure with the Ag film as the substrate and *a*-Si:H as the cover, guided mode can be excited and strongly confined in the AZO layer. The oscillation of field within the AZO layer is also ascribed to the lattice scattering effect. Overall, the enhancement in short wavelength is ascribed to the weakened interference effect, while the hybrid modes consisting of cavity modes, Bloch modes, and plasmonic waveguide modes are responsible to the absorption enhancement at longer wavelengths. The simulated absorptions of *a*-Si:H layers in the planar device and ND device are also plotted in Figure S4. Particularly, the nanopatterned substrate delivers a 2.33-times absorption enhancement near the absorption band edge (λ = 700 nm).

It is worth noting that the nanopatterned substrates with shallow dent (depth ∼200 nm) arrays possess a relatively weaker capacity to trap the light of short wavelengths (<570 nm) in contrast to that of longer wavelengths (>600 nm) as shown in Figure 3, panel d. The 3-D nanostructures with a higher aspect ratio deliver better short wavelength absorption but will simultaneously deteriorate the device electrical performance.[25] Here, the PDMS nanopillar membrane is adopted as an AR layer to capture more incident light without sacrificing the device electrical performance. Note that PDMS is an optically clear, nontoxic material with excellent air and water resistance, which has been widely employed in light-emitting device (LED) and solar cell panel encapsulation. Figure 3, panel c displays the photograph of the nanopatterned device with nanodent covered pillar structure (NDP). It is obviously seen that the device with nanopillars coating appears dark red instead of dark blue due to the suppressed reflection at short wavelengths. A further look at the absorption curve in Figure 3, panel d reflects that the nanopillars coating yields a distinct absorption enhancement in short wavelength region (<570 nm). In this wavelength region, ITO has a reflective index higher than 1.88 (Figure S1a), which leads to a relatively large impedance mismatch from the incident space. The PDMS (refractive index ∼1.4[39]) membrane decorated with nanopillar arrays offers a gradual change of effective refractive index from air to PDMS bulk material that will efficiently suppress the device reflectance.[40] Meanwhile, the simulation results shown in Figure 3, panel e suggest a quite consistent trend with the experimental ones in full wavelength range.

In addition to the optical investigation, the overall electrical performances of the devices on patterned Ti substrates without and with nanopillar coating as well as the planar device as control sample are characterized. Figure 5, panel a depicts the

DOI: 10.1021/acsami.6b02194
ACS Appl. Mater. Interfaces 2016, 8, 10929−10936

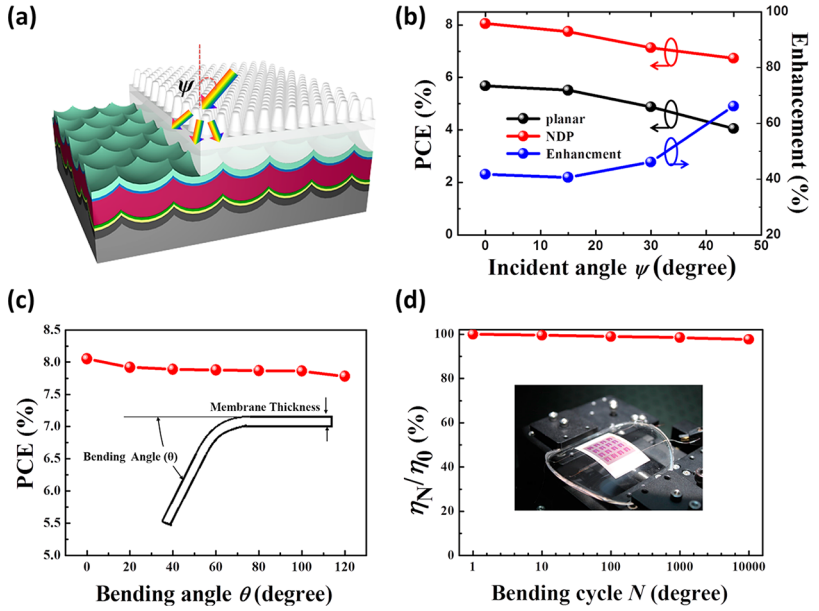

Figure 6. (a) A schematic of defining incident angle. (b) PCE of NDP and planar devices as a function of incident angles as well as the enhancement factors of NDP solar cell with respect to planar device. (c) Efficiency variation of NDP device at different bending angles. (d) Relative efficiencies as a function of bending cycle. The insets in panels c and d represent an illustration of defining bending angle and the measurement setup loaded with a bended device, respectively.

J–*V* characteristics (device active area is 0.12 cm^2) under simulated solar illumination (Newport no. 94063A, 100 mW/cm^2) from a Xe lamp coupled with an air mass 1.5 global (AM 1.5G) filter. The planar device shows comparable performance (PCE = 5.68%) with other literatures.[25,41] In contrast to the planar device, the solar cell on textured Ti substrate represents a much larger short circuit current density (J_{SC} = 13.68 mA/cm^2) due to the optical absorption enhancements. The trend for J_{SC} can be confirmed with external quantum efficiency (EQE) measurements as shown in Figure 5, panel b, which presents a broadband spectra response enhancement with respect to the planar reference device. As a result, the overall performance on patterned Ti substrate is improved from 5.68% to 7.58%. Meanwhile, the almost consistent V_{OC} and *FF* values on nanopatterned devices indicate the high quality film disposition on the shallow nanodent arrays without the deterioration of the internal electric field and carrier collection capability.[18]

The antireflection effect induced by an additional PDMS nanopillar coating is also reflected in the increased J_{SC} (14.60 mA/cm^2) and PCE (8.05%), which are improved by 42.7% and 41.7% over the planar device as shown in Figure 5, panel a. The spectra responses in Figure 5, panel b suggest that the increased photocurrent with the presence of nanopillars is mainly gained from short wavelength below 570 nm that is quite consistent with optical absorption profiles as shown in Figure 3, panel d. A slight increase of V_{OC} is also observed due to the increased J_{SC}.[42] Figure 5, panel c summarizes the J_{SC} and PCE values as a function of device configurations. Each configuration is evaluated at least on four different devices to average out the experimental fluctuation. In conclusion, these results demonstrate that the patterned Ti substrates and antireflective coating thin films can improve the device performance substantially and will have potential applications for other thin-film solar cells based on different material systems.

In practical application of solar panels, the incident angle of solar irradiation changes over time in a day. Therefore, the angular dependent PCE of NDP device together with the planar reference cell is characterized (see Figures 6a,b), where the PCE values are calculated using the device active area, regardless the change of projection area under different incident angles. Benefiting from the dual-layer nanostructure design, the NDP solar cell shows a substantial improvement over all the measured incident angles. Under a 45 deg incident angle, NDP solar cell presents an efficiency of 6.73%, which is 66.17% higher than that of the flat reference device. The omnidirectional improvement on the conversion efficiency is of significance for practical deployment of solar panels without expensive light tracking system.

Previously, we demonstrated flexible solar cells based on aluminum foils, which, however, encountered an efficiency drop up to 7.4% under a 120° bending angle.[20,21] Ti foil substrate, which possesses better flexibility and a higher temperature tolerance, is expected to be an alternative choice for flexible application. Even though Ti in general is more expensive than Al, using thin foil of Ti can help to cut down the cost. To evaluate the variation of performance for the Ti foil based device during flexible operation, the NDP solar cell is measured at different bending angles (Figure 6c), in which the PCE values are calculated using the device active area, regardless of the change of projection area under different bending conditions. The bending angles are automatically controlled using a customized setup as shown in the inset of Figure 6, panel d. The results demonstrate that the efficiency of the NDP device only experienced a marginal drop (3.4%) even at a 120° bending angle. The real time variations of J_{SC} and V_{OC} are also recorded by camera as shown in the Supplementary Videos. Moreover, the robustness of NDP solar cells is tested under repeatedly bending as presented in Figure 6, panel d. The PCE remains as high as 97.6% of the initial efficiency even after 10 000 cycles of bending, as compared with the device performance on Al foils, which retains only 82% of the initial value after 1000 bending cycles.[21] These results demonstrate

DOI: 10.1021/acsami.6b02194
ACS Appl. Mater. Interfaces 2016, 8, 10929–10936

the outstanding flexibility of lightweight titanium foils based photovoltaics.

CONCLUSIONS

Nanopatterned arrays have been demonstrated on highly flexible Ti foils by a low-cost and scalable electrochemical approach. In conjunction with antireflective nanopillar membranes, dual-layer nanopatterned *a*-Si:H TFSCs have been constructed on Ti foils as model devices. It was found that the dual-layer structure resulted in an omnidirectional and broadband enhancement in both optical absorption and quantum efficiency. The improved optical performance is attributed to the gradient in effective refractive index from the top of nanopillar membrane to the bulk PDMS and the hybrid optical modes excited by nanodent back reflector, which was verified by FDTD simulation. A PCE up to 8.05% was achieved, which outperforms the planar counterpart by 41.7%. Moreover, the flexible performances have been studied considering both the bending angle and bending cycles. The Ti foil supported devices presented impressive efficiency retention with 97.6% of the initial value after 10 000 bending cycles. The fabrication processes for both nanotextured Ti foil and polymer nanopillar membrane are compatible with roll-to-roll process, which provide a promising route for large-scale and low-cost production. The technology developed here can be extended to other material systems to enable high performance flexible thin-film photovoltaics.

ASSOCIATED CONTENT

Supporting Information

The Supporting Information is available free of charge on the ACS Publications website at DOI: 10.1021/acsami.6b02194.

Measured refractive index and extinction coefficient of ITO, AZO, and *n-i-p a*-Si:H layers; surface morphology and corresponding height profile of nanotextured Ti substrate; magnetic field distributions in planar device and patterned devices at different wavelengths; simulated absorption spectra of the *a*-Si:H layers in planar and ND solar cells (PDF)

Real time variations of J_{SC} of the NDP device under bending process (AVI)

Real time variations of V_{OC} of the NDP device under bending process (AVI)

AUTHOR INFORMATION

Corresponding Authors

*E-mail: yanxiacui@gmail.com.

*E-mail: lidd@sari.ac.cn.

Author Contributions

¶Y.L. and Z.X. contributed equally to this work.

Notes

The authors declare no competing financial interest.

ACKNOWLEDGMENTS

This work was financially supported by Science & Technology Commission of Shanghai Municipality (Grant No. 14JC1492900), the National Natural Science Foundation of China (Grant No. 61474128, 61475109, 11204205, 11174308, 61274056), the Youth Innovation Promotion Association, Chinese Academy of Sciences (2013302), the Youth Innovation Fund for Interdisciplinary Research of SARI (Y426475234), Hong Kong Innovation Technology Commission project ITS/117/13, and Hong Kong Research Grant Council General Research Fund 612113.

REFERENCES

(1) Espinosa, N.; Hosel, M.; Angmo, D.; Krebs, F. C. Solar Cells With One-day Energy Payback for the Factories of the Future. *Energy Environ. Sci.* **2012**, *5*, 5117−5132.

(2) Hegedus, S. Thin film solar modules: The Low Cost, High Throughput and Versatile Alternative to Si Wafers. *Prog. Photovoltaics* **2006**, *14*, 393−411.

(3) Schubert, M. B.; Werner, J. H. Flexible Solar Cells for Clothing. *Mater. Today* **2006**, *9*, 42−50.

(4) Zhu, J.; Yu, Z. F.; Burkhard, G. F.; Hsu, C. M.; Connor, S. T.; Xu, Y. Q.; Wang, Q.; McGehee, M.; Fan, S. H.; Cui, Y. Optical Absorption Enhancement in Amorphous Silicon Nanowire and Nanocone Arrays. *Nano Lett.* **2009**, *9*, 279−282.

(5) Staebler, D. L.; Wronski, C. R. Reversible Conductivity Changes in Discharge-produced Amorphous Si. *Appl. Phys. Lett.* **1977**, *31*, 292−294.

(6) Yang, J. C. Advances in Amorphous Silicon Alloy Technology-the Achievement of High-efficiency Multijunction Solar Cells and Modules. *Prog. Photovoltaics* **1998**, *6*, 181−186.

(7) Hanak, J.; Korsun, V. Optical Stability Studies of a-Si: H Solar Cells. *Conf. Rec. IEEE Photovoltaic Spec. Conf.*; RCA Laboratories: Princeton, NJ, 1982.

(8) Stuckelberger, M.; Despeisse, M.; Bugnon, G.; Schüttauf, J.-W.; Haug, F.-J.; Ballif, C. Comparison of Amorphous Silicon Absorber Materials: Light-induced Degradation and Solar Cell Efficiency. *J. Appl. Phys.* **2013**, *114*, 154509−154519.

(9) Leung, S.-F.; Zhang, Q.; Xiu, F.; Yu, D.; Ho, J. C.; Li, D.; Fan, Z. Light Management with Nanostructures for Optoelectronic Devices. *J. Phys. Chem. Lett.* **2014**, *5*, 1479−1495.

(10) Haug, F. J.; Ballif, C. Light Management in Thin Film Silicon Solar Cells. *Energy Environ. Sci.* **2015**, *8*, 824−837.

(11) Fan, Z.; Razavi, H.; Do, J.-W.; Moriwaki, A.; Ergen, O.; Chueh, Y.-L.; Leu, P. W.; Ho, J. C.; Takahashi, T.; Reichertz, L. A.; et al. Three-dimensional Nanopillar-array Photovoltaics on Low-cost and Flexible Substrates. *Nat. Mater.* **2009**, *8*, 648−653.

(12) Li, D.; Chang, P.-C.; Chien, C.-J.; Lu, J. G. Applications of Tunable TiO_2 Nanotubes as Nanotemplate and Photovoltaic Device. *Chem. Mater.* **2010**, *22*, 5707−5711.

(13) Wang, X.; Li, Z.; Xu, W.; Kulkarni, S. A.; Batabyal, S. K.; Zhang, S.; Cao, A.; Wong, L. H. TiO_2 Nanotube Arrays based Flexible Perovskite Solar Cells with Transparent Carbon Nanotube Electrode. *Nano Energy* **2015**, *11*, 728−735.

(14) Zhu, J.; Hsu, C.-M.; Yu, Z.; Fan, S.; Cui, Y. Nanodome Solar Cells with Efficient Light Management and Self-Cleaning. *Nano Lett.* **2010**, *10*, 1979−1984.

(15) Hsu, C. M.; Battaglia, C.; Pahud, C.; Ruan, Z.; Haug, F. J.; Fan, S.; Ballif, C.; Cui, Y. High-efficiency Amorphous Silicon Solar Cell on a Periodic Nanocone Back Reflector. *Adv. Energy Mater.* **2012**, *2*, 628−633.

(16) Leung, S.-F.; Yu, M.; Lin, Q.; Kwon, K.; Ching, K.-L.; Gu, L.; Yu, K.; Fan, Z. Efficient Photon Capturing with Ordered Three-dimensional Nanowell Arrays. *Nano Lett.* **2012**, *12*, 3682−3689.

(17) Huang, H.; Lu, L.; Wang, J.; Yang, J.; Leung, S.-F.; Wang, Y.; Chen, D.; Chen, X.; Shen, G.; Li, D.; Fan, Z. Performance Enhancement of Thin-film Amorphous Silicon Solar Cells with Low Cost Nanodent Plasmonic Substrates. *Energy Environ. Sci.* **2013**, *6*, 2965−2971.

(18) Guo, R. C.; Huang, H. T.; Chang, P. C.; Lu, L. F.; Chen, X. Y.; Yang, X. F.; Fan, Z. Y.; Zhu, B. P.; Li, D. D. Coupled Optical and Electrical Modeling of Thin-film Amorphous Silicon Solar Cells based on Nanodent Plasmonic Substrates. *Nano Energy* **2014**, *8*, 141−149.

(19) Xiao, H.; Wang, J.; Huang, H.; Lu, L.; Lin, Q.; Fan, Z.; Chen, X.; Jeong, C.; Zhu, X.; Li, D. Performance Optimization of Flexible A-Si:

H Solar Cells with Nanotextured Plasmonic Substrate by Tuning the Thickness of Oxide Spacer Layer. *Nano Energy* **2015**, *11*, 78−87.
(20) Leung, S. F.; Gu, L.; Zhang, Q.; Tsui, K. H.; Shieh, J. M.; Shen, C. H.; Hsiao, T. H.; Hsu, C. H.; Lu, L.; Li, D.; Lin, Q.; Fan, Z. Roll-to-roll Fabrication of Large Scale and Regular Arrays of Three-dimensional Nanospikes for High Efficiency and Flexible Photovoltaics. *Sci. Rep.* **2014**, *4*, 4243.
(21) Leung, S.-F.; Tsui, K.-H.; Lin, Q.; Huang, H.; Lu, L.; Shieh, J.-M.; Shen, C.-H.; Hsu, C.-H.; Zhang, Q.; Li, D.; et al. Large Scale, Flexible and Three-dimensional Quasi-ordered Aluminum Nanospikes for Thin Film Photovoltaics with Omnidirectional Light Trapping and Optimized Electrical Design. *Energy Environ. Sci.* **2014**, *7*, 3611−3616.
(22) Wang, H.-P.; Lin, T.-Y.; Hsu, C.-W.; Tsai, M.-L.; Huang, C.-H.; Wei, W.-R.; Huang, M.-Y.; Chien, Y.-J.; Yang, P.-C.; Liu, C.-W.; et al. Realizing High-efficiency Omnidirectional N-type Si Solar Cells via the Hierarchical Architecture Concept with Radial Junctions. *ACS Nano* **2013**, *7*, 9325−9335.
(23) Yanagishita, T.; Yasui, K.; Kondo, T.; Kawamoto, Y.; Nishio, K.; Masuda, H. Antireflection Polymer Surface using Anodic Porous Alumina Molds with Tapered Holes. *Chem. Lett.* **2007**, *36*, 530−531.
(24) Tsui, K. H.; Lin, Q.; Chou, H.; Zhang, Q.; Fu, H.; Qi, P.; Fan, Z. Low-cost, Flexible, and Self-cleaning 3D Nanocone Anti-reflection Films for High-efficiency Photovoltaics. *Adv. Mater.* **2014**, *26*, 2805−2811.
(25) Lin, Q. F.; Leung, S. F.; Lu, L. F.; Chen, X. Y.; Chen, Z.; Tang, H. N.; Su, W. J.; Li, D. D.; Fan, Z. Y. Inverted Nanocone-Based Thin Film Photovoltaics with Omnidirectionally Enhanced Performance. *ACS Nano* **2014**, *8*, 6484−6490.
(26) Yu, D. L.; Zhang, S. Y.; Zhu, X. F.; Ma, H. T.; Han, H.; Song, Y. Simulation of Anodizing Current-time Curves and Morphology Evolution of Tio_2 Nanotube Arrays. *J. Solid State Electrochem.* **2014**, *18*, 2609−2617.
(27) Zhong, X.; Yu, D.; Song, Y.; Li, D.; Xiao, H.; Yang, C.; Lu, L.; Ma, W.; Zhu, X. Fabrication of Large Diameter TiO_2 Nanotubes for Improved Photoelectrochemical Performance. *Mater. Res. Bull.* **2014**, *60*, 348−352.
(28) Li, D. D.; Chang, P. C.; Chien, C. J.; Lu, J. G. Applications of Tunable TiO_2 Nanotubes as Nanotemplate and Photovoltaic Device. *Chem. Mater.* **2010**, *22*, 5707−5711.
(29) Odom, T. W.; Love, J. C.; Wolfe, D. B.; Paul, K. E.; Whitesides, G. M. Improved Pattern Transfer in Soft Lithography using Composite Stamps. *Langmuir* **2002**, *18*, 5314−5320.
(30) Palik, E. D. Handbook of Optical Constants. *J. Opt. Soc. Am. A* **1984**, *1*, 1297−1297.
(31) Nagaura, T.; Takeuchi, F.; Inoue, S. Fabrication and Structural Control of Anodic Alumina Films with Inverted Cone Porous Structure using Multi-step Anodizing. *Electrochim. Acta* **2008**, *53*, 2109−2114.
(32) Li, J.; Li, C.; Chen, C.; Hao, Q.; Wang, Z.; Zhu, J.; Gao, X. Facile Method for Modulating the Profiles and Periods of Self-ordered Three-dimensional Alumina Taper-nanopores. *ACS Appl. Mater. Interfaces* **2012**, *4*, 5678−5683.
(33) Su, Z. X.; Zhou, W. Z. Formation Mechanism of Porous Anodic Aluminium and Titanium Oxides. *Adv. Mater.* **2008**, *20*, 3663−3667.
(34) Kim, J.; Battaglia, C.; Charriere, M.; Hong, A.; Jung, W.; Park, H.; Ballif, C.; Sadana, D. 9.4% Efficient Amorphous Silicon Solar Cell on High Aspect-ratio Glass Microcones. *Adv. Mater.* **2014**, *26*, 4082−4086.
(35) Xu, C.; Song, Y.; Lu, L. F.; Cheng, C. W.; Liu, D. F.; Fang, X. H.; Chen, X. Y.; Zhu, X. F.; Li, D. D. Electrochemically Hydrogenated TiO_2 Nanotubes with Improved Photoelectrochemical Water Splitting Performance. *Nanoscale Res. Lett.* **2013**, *8*, 391−397.
(36) Williams, S. S.; Retterer, S.; Lopez, R.; Ruiz, R.; Samulski, E. T.; DeSimone, J. M. High-resolution PFPE-based Molding Techniques for Nanofabrication of High-pattern Density, Sub-20 nm Features: a Fundamental Materials Approach. *Nano Lett.* **2010**, *10*, 1421−1428.
(37) Tian, X. M.; Wang, W. Y.; Hao, Y. Y.; Lin, Y. Y.; Cui, Y. X.; Zhang, Y.; Wang, H.; Wei, B.; Xu, B. S. Omnidirectional and Polarization-insensitive Light Absorption Enhancement in an Organic Photovoltaic Device using a One-dimensional Nanograting. *J. Mod. Opt.* **2014**, *61*, 1714−1722.
(38) Yang, L.; Mo, L.; Okuno, Y.; He, S. Optimal Design of Ultra-broadband, Omnidirectional, and Polarization-insensitive Amorphous Silicon Solar Cells with a Core-shell Nanograting Structure. *Prog. Photovoltaics* **2012**, *21*, 1077−1086.
(39) Llobera, A.; Wilke, R.; Buttgenbach, S. Poly(dimethylsiloxane) Hollow Abbe Prism with Microlenses for Detection based on Absorption and Refractive Index Shift. *Lab Chip* **2004**, *4*, 24−27.
(40) Ji, S.; Song, K.; Nguyen, T. B.; Kim, N.; Lim, H. Optimal Moth Eye Nanostructure Array on Transparent Glass Towards Broadband Antireflection. *ACS Appl. Mater. Interfaces* **2013**, *5*, 10731−10737.
(41) Ram, S. K.; Rizzoli, R.; Desta, D.; Jeppesen, B. R.; Bellettato, M.; Samatov, I.; Tsao, Y. C.; Johannsen, S. R.; Neuvonen, P. T.; Pedersen, T. G.; Pereira, R. N.; Pedersen, K.; Balling, P.; Larsen, A. N. Directly Patterned TiO_2 Nanostructures for Efficient Light Harvesting in Thin Film Solar Cells. *J. Phys. D: Appl. Phys.* **2015**, *48*, 365101−365110.
(42) Ferry, V. E.; Verschuuren, M. A.; Lare, M. C. V.; Schropp, R. E. I.; Atwater, H. A.; Polman, A. Optimized Spatial Correlations for Broadband Light Trapping Nanopatterns in High Efficiency Ultrathin Film a-Si:H Solar Cells. *Nano Lett.* **2011**, *11*, 4239−4245.

DOI: 10.1021/acsami.6b02194
ACS Appl. Mater. Interfaces 2016, 8, 10929−10936